Bol. Grupo Español Carbón

# Impact of hydrothermal pretreatment in acidic medium on the performance of biomass-derived carbons for sodium-ion electrochemical storage

## Impacto del pretratamiento hidrotermal en medio ácido sobre el rendimiento de carbones derivados de biomasa en el almacenamiento electroquímico de iones de sodio

**J.J. Manyà*, D. Alvira, D. Antrorán**

*Aragón Institute for Engineering Research (I3A), Thermochemical Processes Group, University of Zaragoza, Escuela Politécnica Superior, Crta. de Cuarte s/n, 22071 Huesca, Spain*

** joanjoma@unizar.es*

**Abstract**

Hard carbons (HCs) have emerged as promising anode materials for sodium-ion batteries (SIBs) due to their ability to store sodium ions in surface functionalities, structural defects within the amorphous region, pseudographitic domains, and micropores. In this study, HCs were synthesized from vine shoots (VS) and waste hemp hurd (WHH) using a two-step process involving HCl-assisted hydrothermal pretreatment followed by carbonization at 800 °C or 1 000 °C. The resulting HCs demonstrated remarkable electrochemical performance in sodium-ion half-cells, achieving reversible specific capacities of up to 368 mAh $g^{-1}$ at a current density of 0.1 A $g^{-1}$. This excellent behavior is attributed to the appropriate physicochemical properties of the prepared HCs, particularly their hierarchical pore size distribution and tailored carbonaceous structure.

**Resumen**

Los carbones duros (HCs) han surgido como materiales prometedores para su uso como ánodos en baterías de iones de sodio (SIBs). Esto es debido a la capacidad de los HCs para almacenar iones de sodio en grupos funcionales en superficie, defectos estructurales dentro de la región amorfa, dominios pseudo-grafíticos y microporos. En este estudio, se sintetizaron HCs a partir de sarmientos de vid (VS) y residuos de cáñamo industrial (WHH) mediante un proceso en dos etapas que incluye un pretratamiento hidrotermal asistido con HCl seguido de una carbonización a 800 °C o 1000 °C. Los HCs obtenidos demostraron un notable desempeño electroquímico en semiceldas de iones de sodio, alcanzando capacidades específicas reversibles de hasta 368 mAh $g^{-1}$ a una densidad de corriente de 0,1 A $g^{-1}$. Este excelente comportamiento se atribuye a las propiedades fisicoquímicas de los HCs producidos, particularmente a su distribución de tamaños de poro jerarquizada y a su apropiada estructura carbonosa.

### 1. Introduction

Sodium-ion batteries (SIBs) are emerging as leading candidates for the next generation of large-scale electrochemical energy storage systems, essential for integrating intermittent renewable energy sources into the grid [1]. However, their successful deployment hinges on the development of high-capacity anode materials, as traditional graphite anodes exhibit limited sodium-ion storage capacity [2]. Hard carbons (HCs) have gained prominence as promising anode materials for SIBs, thanks to their ability to store sodium ions in surface functionalities, defects in the amorphous region, pseudographitic domains, and micropores [3]. Notably, the production of HCs from biomass waste is gaining attention due to its environmental benefits, cost-effectiveness, and potential to enhance reversible capacities, aligning with circular economy principles.

Sodium insertion into hard carbons primarily occurs in two stages during galvanostatic discharge (see Figure 1): (1) a slope region at relatively high voltage (above 0.15 V) and, (2) a plateau region at low voltage (below 0.15 V) [4]. While the precise mechanisms underlying these regions still remain under scientific debate, a growing consensus suggests that the low- and high-voltage regions are primarily attributed to adsorption-driven storage processes (involving surface charge storage, heteroatoms, and defects) and intercalation and pore filling processes, respectively. However, biomass-derived HCs still present challenges that limit their practical application, including low initial Coulombic efficiency (ICE), limited rate capability, and relativity poor cycling stability. The low ICE is commonly attributed to the formation of a thick solid electrolyte interphase (SEI), particularly when carbonates-based liquid electrolytes are employed, leading to substantial irreversible trapping of sodium ions [5]

Transforming a given biomass precursor into a high-value carbon material can be effectively achieved through hydrothermal pretreatment followed by high-temperature annealing. This approach has been proposed as a facile and environmentally friendly route for synthesizing carbonaceous materials from lignocellulosic feedstocks [6]. Hydrothermal pretreatment utilizes subcritical water as both a solvent and catalyst, enabling acid- and base-catalyzed reactions in biomass conversion. During hydrothermal treatment, cellulose and hemicellulose can hydrolyze above 180 °C into oligomers and

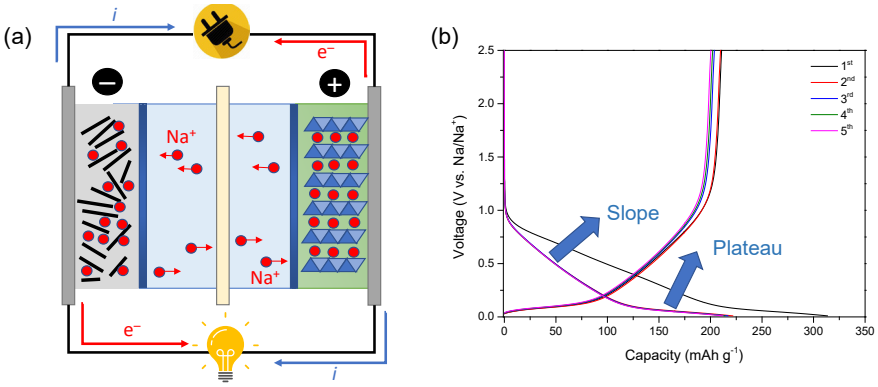


**Figure 1.** Simplified scheme of a sodium-ion battery (a) and typical galvanostatic charge-discharge curves for a HC-based electrode in a half-cell setup (b).

glucose, followed by dehydration, isomerization, and polymerization to form soluble products and hydrochar. Lignin, which is more resistant, partially degrades to phenolic compounds or undergoes solid-state transformations to polyaromatic hydrochar.

Compared with the direct carbonization synthesis pathway, the hydrothermal process fosters pore enlargement and the creation of nanosphere domains, which could enhance the reversible capacity of the resulting HC-based electrodes [7]. Furthermore, using an acidic medium can further catalyze the above-mentioned reactions in biomass precursors, leading to hydrochars with notable chemical, morphological, and structural changes. This opens the door to producing engineered HCs to be used for sodium-ion storage purposes.

This article summarizes the research activities conducted within our research group, focusing on the synthesis of hard carbons derived from two residual biomass sources (vine shots and waste hemp hurd) via hydrothermal pretreatment in acidic medium (HCl) and their subsequent physicochemical characterization and electrochemical performance measurement in sodium-ion half-cells.

## 2. Experimental section

### *2.1. Production of hard carbons*

Two biomass sources were used as carbon precursors: vine shoots (VS) and waste hemp hurd (WHH). VS (*Vitis vinifera L*) were collected in the wine region of Somontano (Huesca, Spain). The raw VS, generated during winter pruning, were sun-dried and crushed to achieve a particle size smaller than 0.7 mm. WHH (*Cannabis sativa L.*), produced in Narlisaray (Black Sea region of Turkey) as a by-product of the hemp defibration process, was sieved to particles approximately 5 mm in length. Results from proximate and elemental analyses, along with the determination of the main biomass constituents (extractives, hemicellulose, cellulose, and lignin) and the primary species present in ash are available in previous publications for VS [8] and WHH [9] samples.

Hard carbons were produced via a two-step carbonization approach. First, 15 g of VS or 5 g of WHH were hydrothermally treated in 50–60 g of a 2 mol $dm^{-3}$ aqueous solution of HCl, for 12 h at 180 °C, using a PTFE-lined stainless-steel autoclave (Huanyu ZHT-172C, 100 mL volume). The material was then collected via vacuum filtration and dried at 100 °C for 12 h. The resulting hydrochar was placed in a ceramic boat and carbonized at a heating rate of 5 °C $min^{-1}$ to final temperatures of 800 °C or 1 000 °C. A tubular reactor made of mullite, inserted into a furnace (Carbolite TF1 16/60/300), was used under an Ar atmosphere. The resulting HCs were ground into powder (particle size below 90 mm), washed with a 2 mol $dm^{-3}$ HCl solution for 2 h at room temperature, and rinsed with DI water until neutral pH was achieved [10,11].

### *2.2. Physicochemical characterization of hard carbons*

The morphologies of the HCs were examined by an Inspect-F50A scanning electron microscope equipped with energy dispersive X-ray spectroscopy (SEM-EDX; FEI, The Netherlands). Further analysis of the HCs structure was conducted with a Tecnai F30 high-resolution transmission electron microscope (HR-TEM, FEI) operated at 300 kV. Interplanar distances were determined from HR-TEM images using Digitalmicrograph® software.

Structural properties were analyzed via X-ray powder diffraction (XRD; Empyrean, Malvern Panalytical, UK, $\lambda$ = 0.154 nm) and Raman spectroscopy (Alpha 300, WITec, Germany, $\lambda$ = 532 nm). The interlayer spacing between graphene layers ($d_{002}$), the apparent thickness of crystallites along the c-axis ($L_c$), and the apparent width of crystallites along the a-axis ($L_a$) were calculated from XRD spectra utilising Bragg's law and Scherrer's equation. Raman spectra were deconvoluted into five peaks, comprising one Gaussian-shaped band (D3) and four Lorentzian-shaped bands (G, D1, D2, and D4). The peak area ratio ($A_{D1}/A_G$) was calculated as a measure of structural disorder.

Specific surface areas and pore size distributions were estimated from $N_2$ and $CO_2$ adsorption isotherms at −196 °C and 0 °C, respectively, following outgassing under vacuum at 150 °C for 8 h. Measurements were conducted using an Autosorb-iQ analyser (Quantachrome, Germany). Specific surface areas (SSA) were calculated using the Brunauer-Emmett-Teller (BET) equation, while pore size distributions were determined using Non-Local Density Functional Theory (NLDFT) models for slit pore geometries. All the calculations were conducted with QuadraWin 6.0 software.

*2.3. Electrochemical measurements*

The electrochemical performance of HCs was evaluated using three-electrode Swagelok t-cells. The working electrode (WE) comprised the respective HC, carbon black Super P™ as a conductive agent, and sodium carboxymethyl cellulose (Na-CMC) as a binder, with mass fractions of 0.8, 0.1, and 0.1, respectively. A uniform slurry was prepared by mixing these components with DI water under magnetic stirring. The slurry was then uniformly applied onto a high-purity aluminum current collector (16 µm thickness) using a baker applicator to form a composite electrode with a thickness of 100 µm. Finally, 12 mm diameter electrodes were punched and dried under vacuum at 120 °C for 12 h [12].

The Swagelok t-cells were assembled in an Ar-filled glovebox (Mbraun, Germany) with $O_2$ and $H_2O$ contents below 0.5 ppm. Two sodium metal discs, with diameters of 12 mm and 5 mm, were used as the counter and reference electrodes, respectively. Two glass fiber filters (190 mm thickness, Prat Dumas, France) served as separator. The electrolyte (200 mL) consisted of a 1 mol $dm^{-3}$ NaTFSI solution in a 1:1 (vol. ratio) mixture of dimethyl carbonate (DMC) and ethylene carbonate (EC).

Electrochemical measurements were performed using a potentiostat-galvanostat (SP-200, Bio-Logic, France) at room temperature. Galvanostatic charge discharge (GCD) measurements were carried out within a potential window of 0.01–2.5 V (vs. $Na^+/Na$).

## 3. Results and discussion

*3.1. Physicochemical properties of hard carbons*

Figure 2 displays SEM images of the produced hard carbons, which have been denoted as function of the precursor (VS or WHH), hydrothermal medium (water, *w*, or *HCl*), and highest annealing temperature (800 or 1 000 °C). As observed in Figure 2, all the produced HCs preserved the biomass' structural voids and channels, likely due to the relatively high lignin contents (20.3 % [8] and 23.8 % [9] by mass for VS and WHH, respectively). This preservation may enhance electrolyte penetration and sodium-ion diffusion, potentially improving electrochemical performance. Additionally, HCl-assisted hydrothermal pretreatment led to carbon surfaces with rougher textures and smoother contours, attributed to the promoted hydrolysis of soluble compounds. When HCs were produced at a highest temperature of 1 000 °C, randomly distributed microsphere domains—particularly in WHH-HCl-1000—were observed.

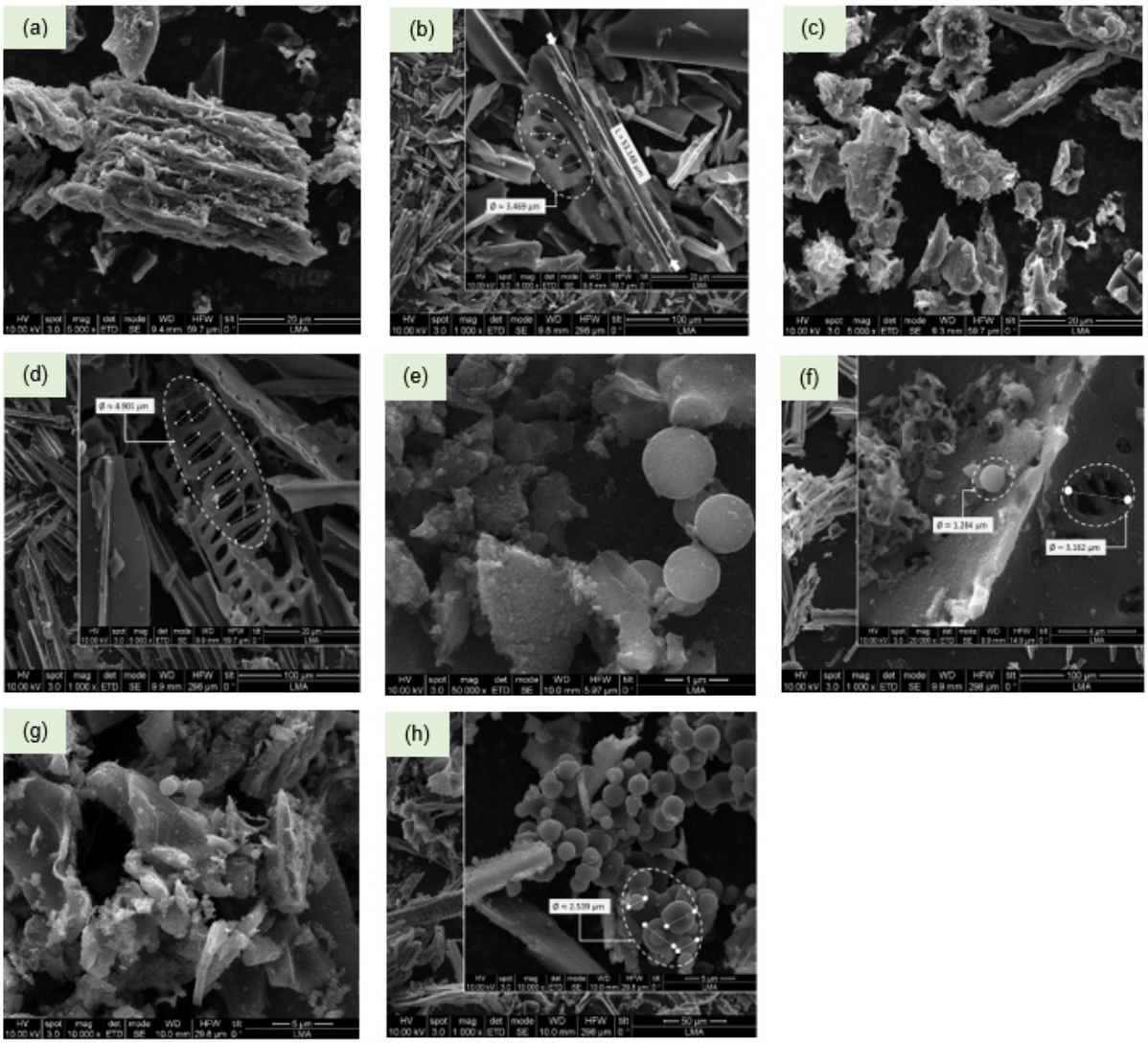


**Figure 2.** SEM images of VS-w-800 (a), WHH-w-800(b), VS-w-1000 (c), WHH-w-1000 (d), VS-HCl-800 (e), WHH-HCl-800 (f), VS-HCl-1000 (g), and WHH-HCl-1000 (h).

The acquired HR-TEM images (see Figure 3) revealed that the hard carbons obtained through hydrothermal pretreatment with pure water exhibited a predominantly amorphous structure with randomly oriented pseudographitic domains. Furthermore, $d_{002}$ values exceeding 0.36 nm were observed, enabling Na-ion intercalation. An increase in the temperature from 800 °C to 1000 °C enhanced the formation of curved graphene-like layers around closed or quasi-closed pores, which are hypothesized to improve the specific capacity of the active material [13]. When HCl was employed during the hydrothermal pretreatment, similar or even wider interlayer spacings—ranging from 0.41 nm to 0.49 nm (as shown in Figures 3e, 3f, and 3h)—were observed. Following annealing at 1 000 °C, while amorphous regions with turbostratic domains persisted ($d_{002} \simeq 0.40$ nm), other local domains underwent significant ordering, resulting in fully graphitic zones with $d_{002}$ values below 0.30 nm (see Figure 3g).

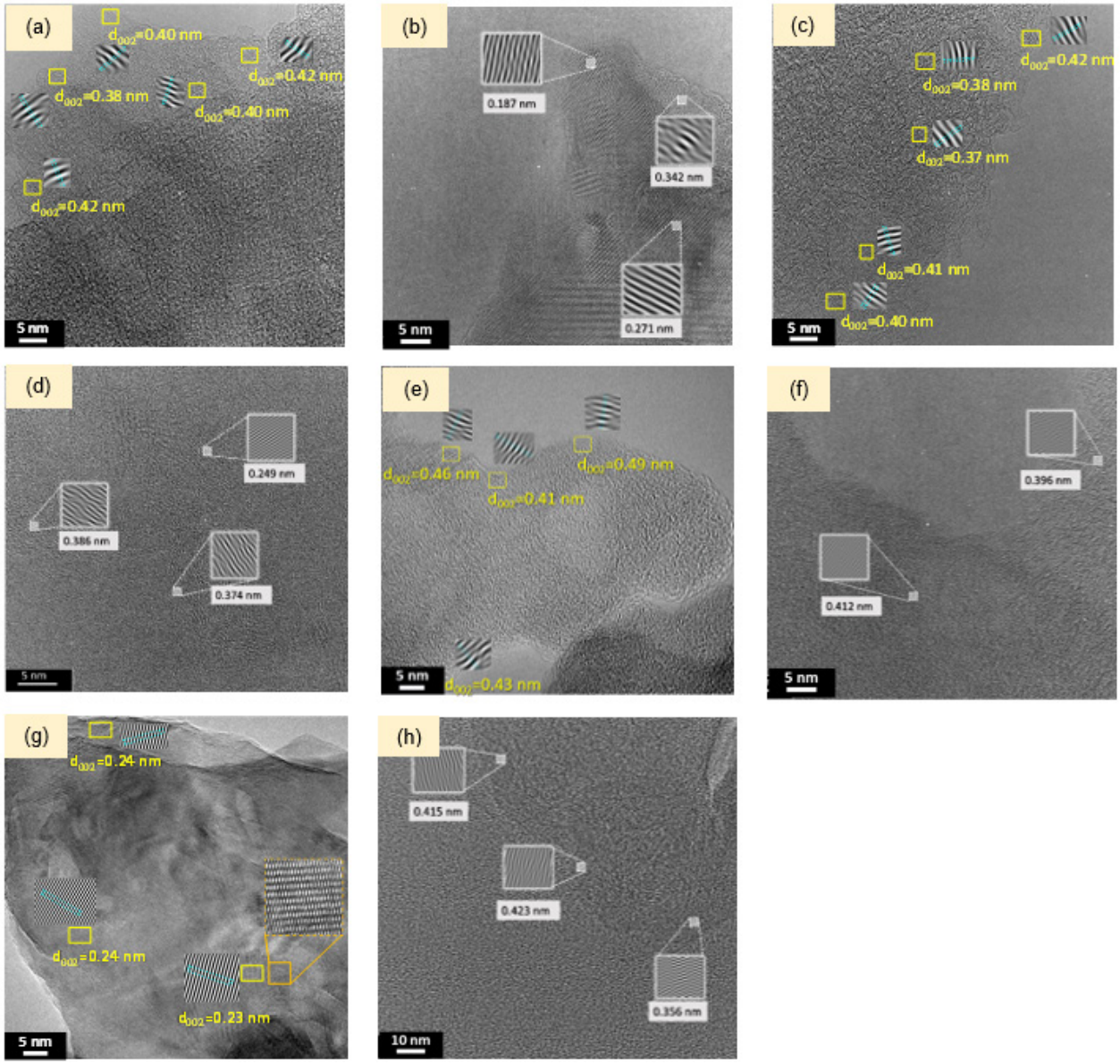


**Figure 3.** HR-TEM images of VS-w-800 (a), WHH-w-800(b), VS-w-1000 (c), WHH-w-1000 (d), VS-HCl-800 (e), WHH-HCl-800 (f), VS-HCl-1000 (g), and WHH-HCl-1000 (h).

Despite the differences observed in the structural ordering on surface, results from XRD and Raman spectroscopy (see Table 1) indicate that the degree of disorder for bulk materials was relatively similar among them, except for VS-w-800, which appears to exhibit a high degree of disorder. For VS-derived HCs, however, a slight increase in structural order is deduced in carbons annealed at higher temperature and/or hydrothermally treated with HCl instead of water.

Regarding the textural features of hard carbons, Table 2 lists the specific surface areas and pore volumes determined from $N_2$ and $CO_2$ adsorption isotherms. The specific surface areas significantly increased when the hydrothermal pretreatment was performed in an acidic medium. For VS-derived carbons, relatively high mesopore volumes were obtained at both annealing temperatures. These hierarchical pore size distributions could shorten the diffusion paths for Na-ions and enhance kinetics [14].

**Table 1.** Structural parameters of hard carbons deduced from XRD and Raman analyses.

| Material | From XRD | | | From Raman |
|---|---|---|---|---|
| | $d_{002}$ (nm) | $L_c$ (nm) | $L_a$ (nm) | $A_{D1}/A_G$ |
| VS-w-800 | 0.385 | 0.887 | 2.875 | 8.05 ± 0.04 |
| WHH-w-800 | 0.388 | 0.895 | 3.508 | 4.79 ± 0.30 |
| VS-w-1000 | 0.381 | 0.874 | 3.822 | 5.69 ± 0.22 |
| WHH-w-1000 | 0.381 | 0.874 | 4.009 | 5.22 ± 0.46 |
| VS-HCl-800 | 0.374 | 0.922 | 3.334 | 5.44 ± 0.41 |
| WHH-HCl-800 | 0.385 | 0.880 | 3.300 | 4.05 ± 0.55 |
| VS-HCl-1000 | 0.373 | 1.011 | 3.784 | 4.76 ± 0.25 |
| WHH-HCl-1000 | 0.383 | 0.868 | 3.451 | 5.52 ± 0.50 |

**Table 2.** Textural features deduced from $N_2$ and $CO_2$ adsorption isotherms.

| Material | $S_{BET}$[a] ($m^2\ g^{-1}$) | $S_{BET}$[b] ($m^2\ g^{-1}$) | Micropore volume[c] ($cm^3\ g^{-1}$) | Mesopore volume[c] ($cm^3\ g^{-1}$) | Ultramicropore volume[d] ($cm^3\ g^{-1}$) |
|---|---|---|---|---|---|
| VS-w-800 | 82.0 | 397 | 0.080 | 0.025 | 0.122 |
| WHH-w-800 | 61.7 | 388 | 0.031 | 0.007 | 0.180 |
| VS-w-1000 | 17.0 | 445 | 0.062 | 0.030 | 0.127 |
| WHH-w-1000 | 11.1 | 402 | 0.006 | 0.011 | 0.186 |
| VS-HCl-800 | 659 | 575 | 0.295 | 0.240 | 0.157 |
| WHH-HCl-800 | 462 | 423 | 0.178 | 0.030 | 0.196 |
| VS-HCl-1000 | 127 | 440 | 0.079 | 0.212 | 0.127 |
| WHH-HCl-1000 | 95.6 | 428 | 0.058 | 0.011 | 0.199 |

[a] From $N_2$ adsorption isotherm at –196 °C. [b] From $CO_2$ adsorption isotherm at 0 °C. c From N2 adsorption data using a NLDFT model. d From $CO_2$ adsorption data using a NLDFT model.

### *3.2. Electrochemical performance of hard carbon-based anodes*

Table 3 presents the charge specific capacities and the corresponding ICE values derived from GCD measurements (over the first five cycles) at a relatively low current density (0.1 mA $g^{-1}$). The WHH-HCl-1000-based electrode exhibited excellent performance, achieving a specific capacity of 368 mAh $g^{-1}$ in the fifth cycle. This value is significantly higher than those reported at the same current density for other biomass-derived HCs prepared via hydrothermal pretreatment and thermal annealing [15,16]. The remarkable capacities and relatively high ICE value achieved for WHH-HCl-1000 can be attributed to its structural and textural characteristics, which offer numerous active sites for reversible Na-ion storage through adsorption on defects, micropore filling, and intercalation. The low ICE values measured for the rest of carbons obtained via HCl-assisted hydrothermal pretreatment can be ascribed to the presence of relatively high volumes of mesopores and/or wide micropores, which promote the formation of thick SEI layers when carbonates-based electrolytes are employed [12].

**Table 3.** TCharge specific capacities (mAh $g^{-1}$) and ICE values from the first five discharge-charge cycles at 0.1 mA $g^{-1}$.

| Material | Capacity at cycle 1 | Capacity at cycle 2 | Capacity at cycle 3 | Capacity at cycle 4 | Capacity at cycle 5 | ICE (%) |
|---|---|---|---|---|---|---|
| VS-w-800 | 162 | 160 | 157 | 153 | 149 | 56 |
| WHH-w-800 | 101 | 99 | 98 | 97 | 96 | 48 |
| VS-w-1000 | 246 | 243 | 239 | 237 | 236 | 71 |
| WHH-w-1000 | 212 | 200 | 191 | 187 | 185 | 75 |
| VS-HCl-800 | 192 | 188 | 187 | 186 | 183 | 34 |
| WHH-HCl-800 | 162 | 161 | 160 | 159 | 158 | 39 |
| VS-HCl-1000 | 167 | 164 | 161 | 159 | 158 | 39 |
| WHH-HCl-1000 | 385 | 381 | 372 | 368 | 368 | 69 |

Regarding the rate capability of the HC-based electrodes, Figure 4 displays the charge specific capacities derived from GCD measurements conducted at current densities of 0.1, 0.5, 1, and 2 A $g^{-1}$. Among the carbons synthesized from VS, VS-HCl-800 exhibited the highest rate capability, with reversible capacities of 146, 126, and 102 mAh $g^{-1}$ when cycled at 0.5, 1, and 2 A $g^{-1}$, respectively. This finding can be attributed to the hierarchical pore size distribution of this material, which includes a relatively high mesopore volume (see Table 2). In contrast, the best-performing material at 0.1 A $g^{-1}$ (WHH-HCl-1000) showed a significant decline in charge capacity when cycled at higher current rates, delivering 156, 115, and 83 mA h $g^{-1}$ at 0.5, 1, and 2 A $g^{-1}$, respectively.

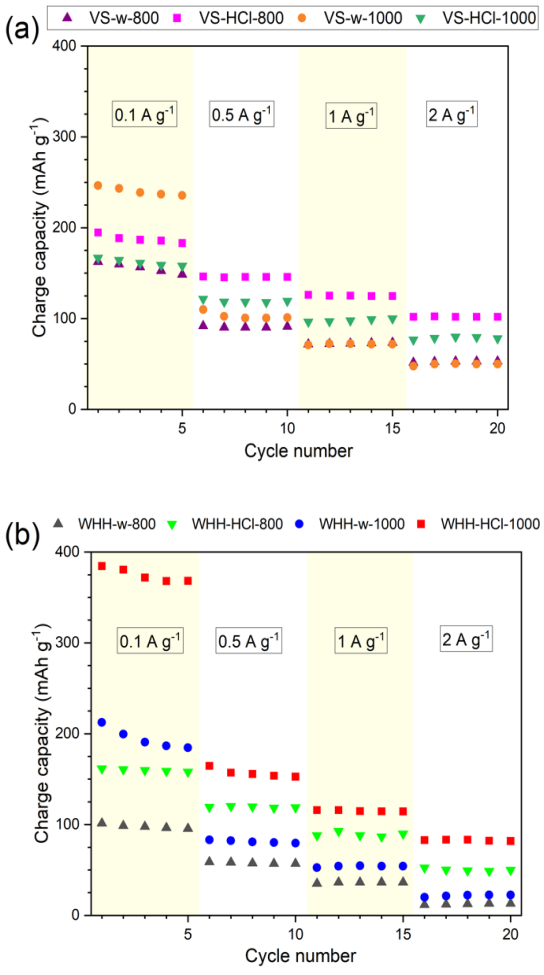


**Figure 4.** Charge specific capacities vs. cycle number at various current densities ranging from 0.1 to 2 A $g^{-1}$ for (a) VS-derived HCs, and (b) WHH-derived HCs.

To evaluate the cycling stability of VS-HCl-800- and WHH-HCl-1000-based electrodes, 300 discharge-charge cycles were performed at 1 A $g^{-1}$, following an initial set of five cycles at 0.1 A $g^{-1}$. As shown in Figure 5, both electrodes exhibited a persistent decline in charge capacity over the cycles, likely due to the extent of parasitic reactions and/or the relatively thick and nonuniform SEI [17]. Nevertheless, upon restoring the current rate to its initial value (0.1 A $g^{-1}$), the WHH-HCl-1000 electrode demonstrated a satisfactory capacity retention of 91 % relative to the values measured during the first five cycles at the same current rate. In contrast, the VS-derived electrode exhibited a lower retention of 79 % under the same conditions.

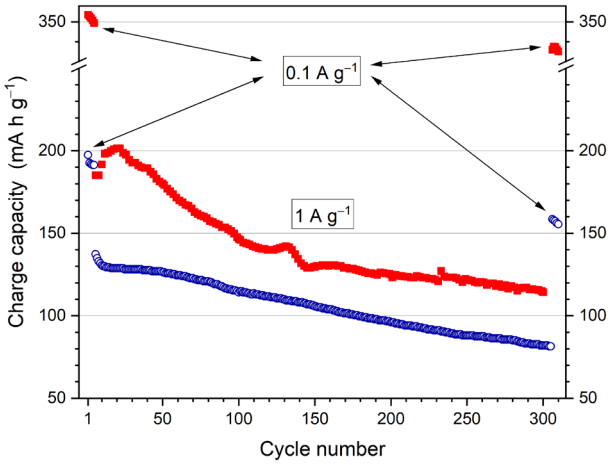


**Figure 5.** Cycling performance of VS-HCl-800 (blue circles) and WHH-HCl-1000 (red squares) at 1 A $g^{-1}$

## 4. Conclusions

The results of this study confirm the potential of hard carbons derived from two waste biomass sources as anode materials for SIBs. Moreover, the proposed synthesis pathway presents a promising alternative to other approaches reported in the literature, offering advantages in terms of energy consumption and scalability.

The superior performance of the hard carbons pretreated hydrothermally in a hydrochloric acid medium can be attributed to their hierarchical pore size distribution, which facilitates Na-ion diffusion, and their appropriate carbon structure. This structure combines a highly disordered amorphous phase (with enlarged interlayer spacings) with highly graphitized microdomains, providing numerous active sites for Na-ion intercalation and simultaneously enhancing ionic conductivity.

Nevertheless, further research is still required to address the limitations identified in the present study, particularly the relatively poor cycling stability observed for the HC-based electrodes. In this regard, enhancing the performance of the electrode-electrolyte interphase is essential and could be achieved by developing more efficient electrolyte formulations.

## References

[1] Nayak PK, Yang L, Brehm W, Adelhelm P. From Lithium-Ion to Sodium-Ion Batteries: Advantages, Challenges, and Surprises. Angew Chem, Int Ed 2018; 57: 102–120.

[2] Xu ZL, Yoon G, Park KY, Park H, Tamwattana O, Joo Kim S, et al. Tailoring sodium intercalation in graphite for high energy and power sodium ion batteries. Nat Commun 2019; 10: 2598.

[3] Matei Ghimbeu C, Beda A, Réty B, El Marouazi H, Vizintin A, Tratnik B, et al. Review: Insights on Hard Carbon Materials for Sodium-Ion Batteries (SIBs): Synthesis – Properties – Performance Relationships. Adv Energy Mater 2024; 14: 2303833.

[4] Alvira D, Antorán D, Manyà JJ. Plant-derived hard carbon as anode for sodium-ion batteries: A comprehensive review to guide interdisciplinary research. Chem Eng J 2022; 447: 137468.

[5] Kulova TL, Skundin AM. Electrode/Electrolyte Interphases of Sodium-Ion Batteries. Energies 2022, 15: 8615.

[6] Nicolae SA, Au H, Modugno P, Luo H, Szego AE, Qiao M, et al. Recent advances in hydrothermal carbonisation: From tailored carbon materials and biochemicals to applications and bioenergy. Green Chemistry 2020; 22: 4747–4800.

[7] Wang J, Yan L, Ren Q, Fan L, Zhang F, Shi Z. Facile hydrothermal treatment route of reed straw-derived hard carbon for high performance sodium ion battery. Electrochim Acta 2018; 291: 188–196.

[8] Alvira D, Antorán D, Vidal M, Sebastian V, Manyà JJ. Vine Shoots-Derived Hard Carbons as Anodes for Sodium-Ion Batteries: Role of Annealing Temperature in Regulating Their Structure and Morphology. Batter Supercaps 2023; 6: e202300233.

[9] Antorán D, Alvira D, Peker ME, Malón H, Irusta S, Sebastián V, et al. Waste Hemp Hurd as a Sustainable Precursor for Affordable and High-Rate Hard Carbon-Based Anodes in Sodium-Ion Batteries. Energy Fuels 2023; 37: 9650–9661.

[10 Antorán D, Alvira D, Sebastián V, Manyà JJ. Enhancing waste hemp hurd-derived anodes for sodium-ion batteries through hydrochloric acid-mediated hydrothermal pretreatment. Biomass Bioenergy 2024; 184: 107197.

[11] Alvira D, Antorán D, Darjazi H, Elia GA, Sebastian V, Manyà JJ. Sustainable conversion of vine shoots and pig manure into high-performance anode materials for sodium-ion batteries. J Power Sources 2024; 614: 235043.

[12] Alvira D, Antorán D, Darjazi H, Elia GA, Gerbaldi C, Sebastian V, et al. High performing and sustainable hard carbons for Na-ion batteries through acid-catalysed hydrothermal carbonisation of vine shoots. J Mater Chem A 2025; Advance article.

[13] Chen D, Zhang W, Luo K, Song Y, Zhong Y, Liu Y, et al. Hard carbon for sodium storage: Mechanism and optimization strategies toward commercialization. Energy Environ Sci 2021; 14: 2244–2262.

[14] Huang S, Lv Y, Wen W, Xue T, Jia P, Wang J, et al. Three-dimensional hierarchical porous hard carbon for excellent sodium/potassium storage and mechanism investigation. Mater Today Energy 2021; 20: 100673.

[15] Zhu Z, Zeng X, Wu H, Wang Y, Cheng H, Dong P, et al. Green energy application technology of litchi pericarp-derived carbon material with high performance. J Clean Prod 2021; 286: 124960.

[16] Wang J, Yan L, Ren Q, Fan L, Zhang F, Shi Z. Facile hydrothermal treatment route of reed straw-derived hard carbon for high performance sodium ion battery. Electrochim Acta 2018; 291: 188–196.

[17] Hirsh HS, Sayahpour B, Shen A, Li W, Lu B, Zhao E, et al. Role of electrolyte in stabilizing hard carbon as an anode for rechargeable sodium-ion batteries with long cycle life. Energy Storage Mater 2021; 42: 78–87.